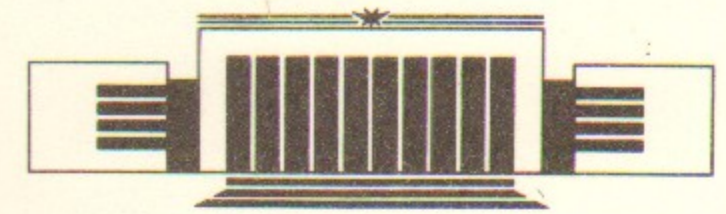33

ИЯФ

ИНСТИТУТ ЯДЕРНОЙ ФИЗИКИ СО АН СССР

M. Carter, D. Behne, S. Hulsey, A. Molvik, G. Porter,
Y. Belchenko, E. Gilev, V. Davydenko, G. Dimov,
V. Dudnikov, A. Kabantsev, V. Karliner, I. Morozov,
V. Sokolov, S. Taskaev, G. Fixel, V. Chupriyanov

EXPERIMENTS WITH THE TIME-OF-FLIGHT NEUTRAL PARTICLE ANALYZER ON AMBAL-U

Experiments with the Time-of-Flight Neutral Particle Analyzer on AMBAL-U

M.Carter, D.Behne, S.Hulsey, A.Molvik, G.Porter

Lawrence Livermore National Laboratory
Livermore, California, USA

Y.Belchenko, E.Gilev, V.Davydenko, G.Dimov,
V.Dudnikov, A.Kabantsev, V.Karliner, I.Morozov,
V.Sokolov, S.Taskaev, G.Fixel, V.Chupriyanov

Institute of Nuclear Physics
630090, Novosibirsk, USSR

ABSTRACT

Experiments with a Time-of-Flight neutral particle analyzer on the device AMBAL-U of the Institute of Nuclear Physics of the Siberian Branch of the USSR Academy of Sciences were performed during the period June to August, 1987. The Time-of-Flight analyzer has been developed at the Lawrence Livermore National Laboratory and was used earlier in experiments on TMX-U. The results of the study of the target plasma generated by plasma guns and the characteristics of the plasma during neutral beam injection are presented here.

1. DESCRIPTION OF AMBAL-U INSTALLATION

1.1. General Review

The AMBAL-U device is a classical mirror with minimum-B that was assembled in 1986 from the components of the ambipolar trap AMBAL [1]. AMBAL-U is currently being used for studies of high-temperature plasmas obtained by neutral-beam injection. Present studies concentrate on obtaining optimal conditions for the capture of energetic neutral particles and the accumulation of hot ions in the magnetic trap.

Figs 1, 2 show the magnet system, the plasma configuration, the devices for plasma production, and various diagnostics.

The AMBAL-U magnet system consists of two Yin-Yang type coils. The magnetic field in the center of the trap is variable up to 10 kG. The mirror ratio in the trap is 2. The distance between the magnetic mirrors is 1 meter. The opening in the vacuum chamber for the plasma is 42 cm in diameter at the midplane of the trap. At the peak of the mirror, the opening is rectangular in shape with size 9×120 cm. The designed plasma diameter at the midplane of the trap is 22 cm.

The high vacuum pumping system consists of turbomolecular and ion pumps, cryopanels and titanium getters. After heating the entire AMBAL-U vacuum system to 400°C and depositing fresh titanium, the base pressure in the AMBAL-U vacuum system can be as low as 5×10^{-9} Torr.
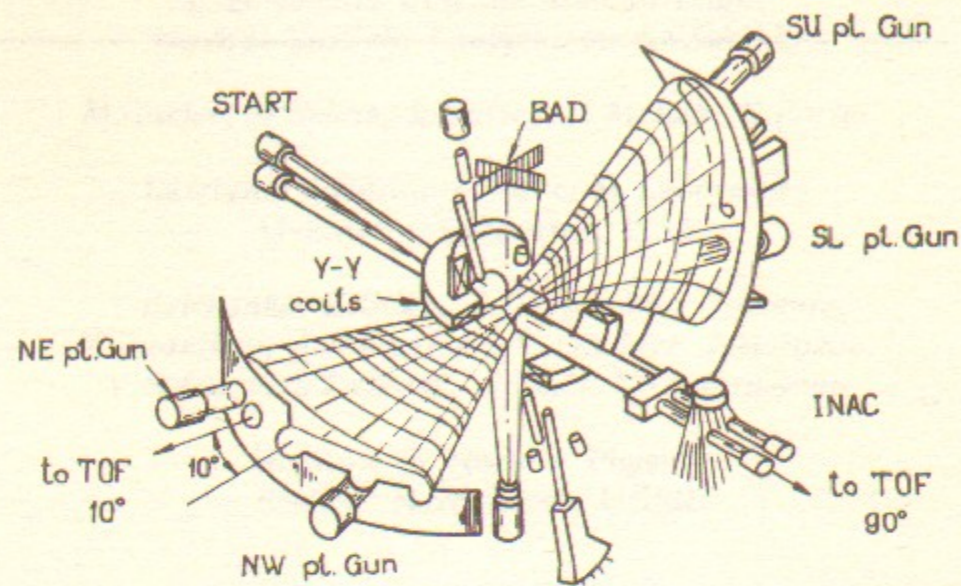
Fig. 1. Schematic diagram of the AMBAL-U device showing the magnet configuration, the location of the START and INAK injectors, the four plasma guns and various diagnostics.
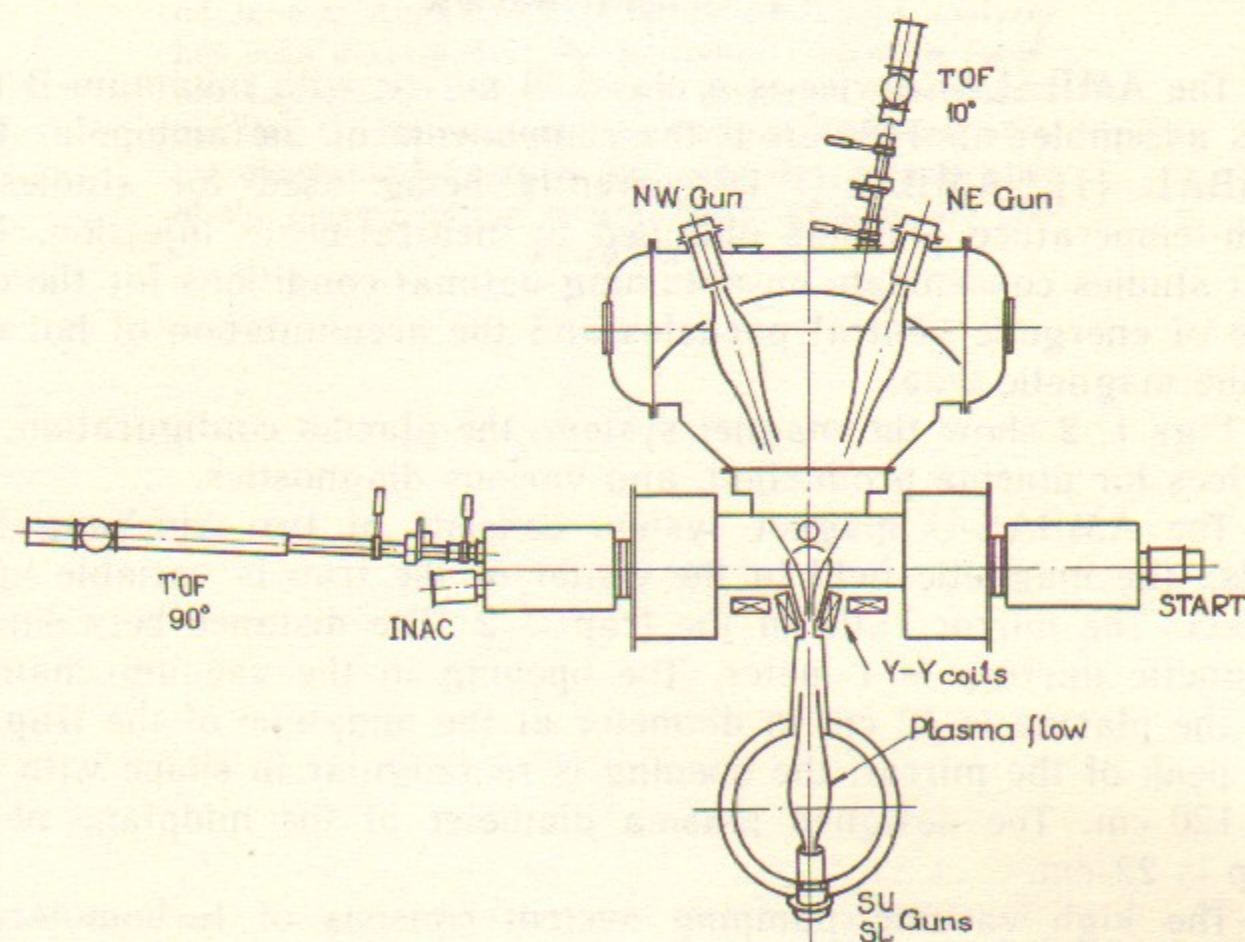

Fig. 2. Top view of the AMBAL-U facility showing the START injectors, INAK injectors, plasma guns and the two locations of the TOF analyzer.

Four plasma guns are located behind the plasma receiver plates on the end walls of the device. Target plasma density above 10^{13} cm^{-3} was generated.

Two short pulse neutral beam injectors (START) are located on the east vacuum tank (right one in Fig. 2). Two quasi-stationary injectors (INAK) are located on the opposite side. In the present experiment we used only single INAK.

Various diagnostics including the two locations of the Time-of-Flight analyzer are also shown in Fig. 1. A schematic diagram of the AMBAL-U installation is shown in Fig. 2 also. This figure shows AMBAL-U as viewed from the top.

1.2. Plasma Production System

The initial target plasma in AMBAL-U is generated by firing gas discharge plasma guns [2, 3]. Each gun generates a hollow cylindrical stream with the initial outer diameter 13 cm and thickness ~1 cm. The total ion current is 2—3 kA. In order to match the magnetic field flux outgoing from the gun discharge washer channel with the given plasma shape in the midplane of the trap, each gun was installed inside the pulse solenoid with the field up to 0.6 T. So the plasma size increases substantially when passing through the low field fan region and then decreases again in the mirror.

Fig. 3 shows the calculated plasma cross section at the midplane of the trap for $B_{mid} = 7.5$ kG and $B_{sol} = 5.0$ kG. Preliminary measurements performed on a test stand and on AMBAL-U have shown that the exter-

Fig. 3. Cross section of the plasma shape at the midplane of AMBAL-U.

nal boundary of the stream plasma follows the magnetic flux tube, but after passing the mirror the internal cavity of the stream plasma is filled with plasma by anomalous diffusion [4, 5]. The plasma gun parameters are optimized by varying the amount of gas, the time delay between the gas pulse and the discharge, and the solenoid field.
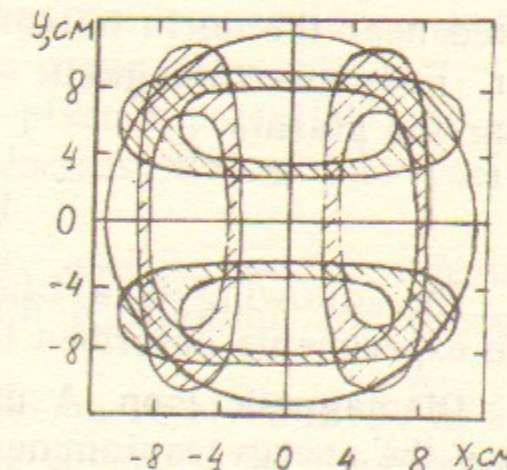
1.3. Beam Injection System

The neutral beams we used were generated by two START and one INAK injectors.

The START injector [6] has output current up to 80 A at 20 kV. The pulse duration is 250 μs. The fraction of full energy neutrals extracted from the beam is 95%. The diameter of the plasma emission surface is 13 cm. The angular divergence of the beam is $0.7 \times 1.4°$. The maximum total flux of accelerated atoms incident on the target plasma is about 120 atom Amperes. The dimensions of the beam ($1/e$ width) incident on the plasma is 16×24 cm. The plasma volume illuminated by the beam is approximately 8 liters.

A quasi-stationary injector INAK is described in [7]. Ion beams with energy of 25 keV and current of 25 A have been obtained on a test stand. The maximum pulse duration is .1 s. The fraction of full energy neutrals is 90%. The angular spread of the INAK beam is $.5 \times 1.0°$. The beam dimensions ($1/e$ width) at the plasma are 15×23 cm. The expected flux of neutrals incident on the plasma is 15—20 atom Amperes per beam.

In some shots we made a hydrogen puffing with the gas box located near the north mirror on the upper wall of the vacuum chamber. Fast electromagnetic valve was used to inject additional gas near the plasma.

1.4. Diagnostics

The following is a brief description of the diagnostics used in the experiments described in this paper.

Diamagnetic loop. A diamagnetic loop (DML) is used to measure the energy containment of the plasma. The shape and location of the DML were chosen to minimize the sensitivity to the plasma currents flowing in the target plasma streams.

Multicord hydrogen beam probe. The radial profile of the line density at the midplane of the trap is measured with a multicord (10 channel) beam attenuation diagnostic. The diagnostic beam is a 10 keV, 1 A neutral source.

Microwave cutoff diagnostic. The maximum plasma density is measured at the midplane of the trap using two microwave cutoff diagnostics. The wavelength of the microwaves is 4 and 8 mm, corresponding to a cutoff density of $7 \times 10^{13} cm^{-3}$ and $1.7 \times 10^{13} cm^{-3}$.

Five-channel electrostatic charge-exchange analyzer. The energy spectrum of the charge exchange atoms emitted from the midplane of the trap is measured. The line of sight of the analyzer is directed perpendicular to the beam injection.

H-alpha and H-beta light detectors. The intensity of the H_α and H_β radiation from the midplane of the trap is monitored with light sensitive detectors.

Langmuir probes. Two movable triple Langmuir probes are used, one in each fan tank to monitor the density and electron temperature of the stream plasma.

RF loop probes. Several RF loop probes are used to monitor the plasma for evidence of MHD instabilities and microinstabilities.

Floating potential probes. Several multitip floating potential probes are used to monitor the plasma for high frequency RF activity.

Fast ion gauges. Specially shielded ion gauges with time response of about .5 ms are used to measure the neutral pressure near the plasma surface.

Argon beam probe. Electron temperature measurements are made at the midplane of the trap by measuring the attenuation of an energetic neutral argon beam. The electron temperature can be determined by the ratio of the hydrogen to argon attenuation.

Electrostatic end-loss analyzers. The plasma potential and ion temperature can by determined with the electrostatic end-loss analyzers located on the end walls of the device.

Pyroelectric bolometers. Bolometers are used to monitor the total power radiated from the plasma including radiation and charge exchange flux.

End wall diagnostics. A segmented plasma receiver array is located in each end tank. Each set of plates consists of 10 segments. The receiver plates can either be floated through a 10 kΩ resistance and the floating potential recorded or grounded and the net plasma current recorded.

Time-of-Flight neutral particle analyzer. A Time-of-Flight neutral particle analyzer is used to measure the energy spectrum of the low energy neutrals ($E < 1.5$ keV) emitted from the plasma. The analyzer has been used in two locations on AMBAL-U, 10 and 90°.

1.4.1 The Time-of-Flight Neutral Particle Analyzer

The Time-of-Flight (TOF) neutral particle analyzer is used to measure the velocity distribution of the charge exchange neutral

particles emitted from the plasma. The TOF analyzer, shown in Fig. 4, consists of a high speed rotating chopper, a 4 meter flight
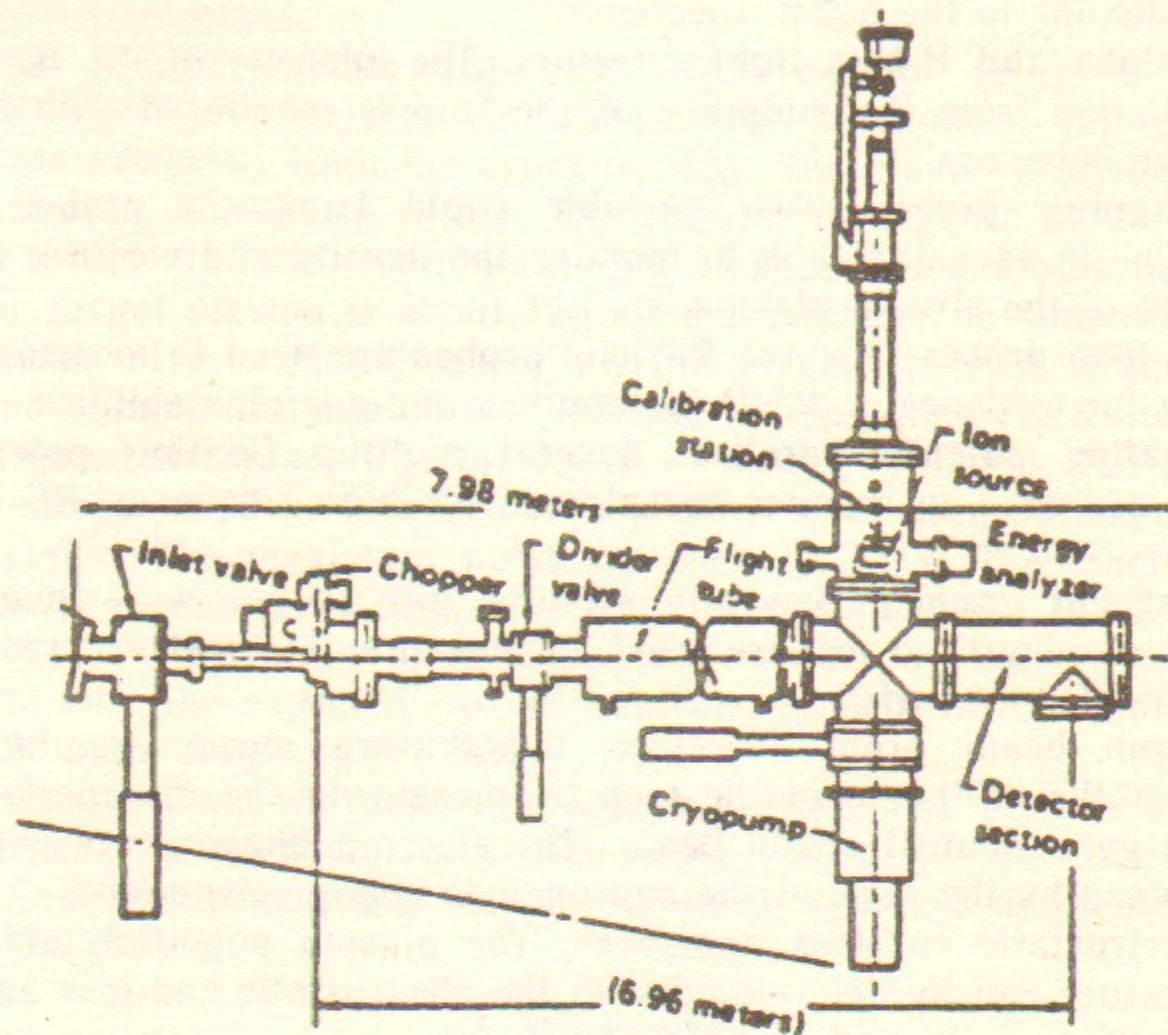

Fig. 4. Diagram of the TOF analyzer used on AMBAL-U.

tube, and a secondary emission type neutral particle detector. The chopper separates the emitted neutral flux into small packets of particles. As these particles traverse the flight tube, they disperse in time. From the time dependence of the detected signal, the velocity distribution of the neutral particles can be determined. The chopper disk has 14 equally-spaced tapered slots. Each slot is .025 cm wide (at the outer edge) and 4 cm long. A stationary slit, located just beyond the chopper disk is identical in shape to each of the rotating slits. At the highest chopper rotational speed (710 Hz), the slit open time is 1 μs. For a more complete description of the TOF analyzer, the reader is referred to the TMX-U Final Report [8] or the Ph. D. thesis by Carter [9].

The energy resolution of the TOF analyzer is determined by the ratio of the particle flight time and the slit open time. The energy resolution, $\Delta E/E$, for hydrogen neutrals is better than 10% for par-

8

ticle energies less than 1 keV. The time resolution of the TOF plasma measurements is determined by the rotational speed of the particle chopper. Typically, the TOF measures the velocity distribution of the emitted neutrals once every 100 μs. Fig. 5 shows a typical detector signal versus time. The initial peak in the signal is due to plasma light. The energy of the detected particles can be determined
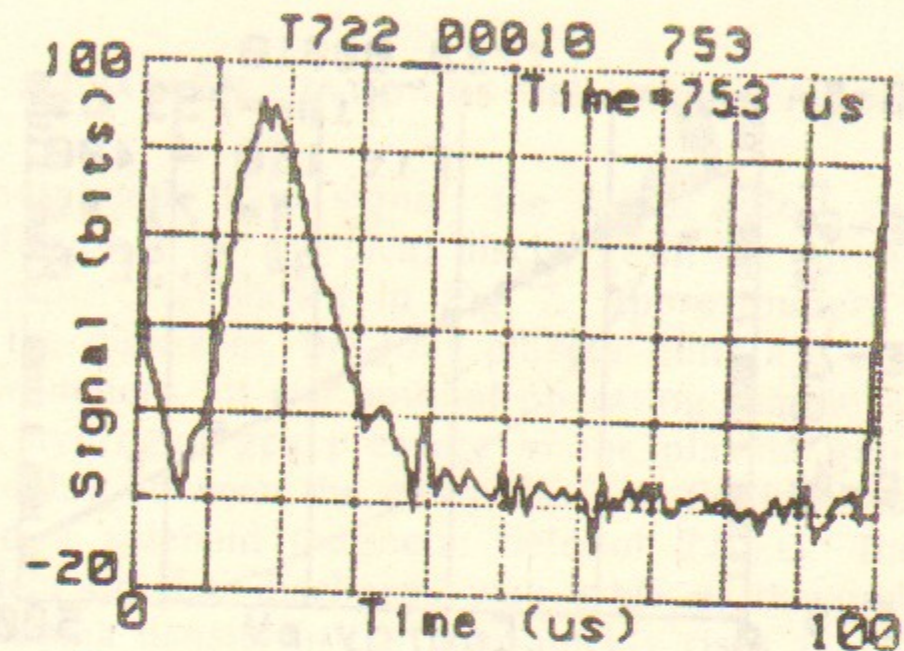

Fig. 5. Typical TOF detector signal versus time.

by measuring the time between the arrival of the light and the particles. We must include variations in the sensitivity of the analyzer versus the energy of the incident particles to calculate the velocity distribution function of the emitted neutrals from the detector signal. It has been shown [2] that the analyzer sensitivity varies as the 7/2 power of the particle energy for the case of charge exchange of plasma ions with high energy neutral beams. This assumes the charge exchange cross section is independent of the energy of the plasma ions (a reasonable assumption for energies below 1 keV). In the case of charge exchange with background gas, variations in the charge exchange cross section with energy should also be included. The charge exchange cross section has been shown to decrease approximately with the ion energy to the 1/4 power [11]. In the case of charge exchange of plasma ions with cold neutral gas, the ion distribution function, $f(E)$, can be obtained from the detector signal, $S(T)$, by the equation

$$S(t) = f(E)\,E^{13/4}. \tag{1}$$

9

where E is the energy of the incident ions, $1/2mv^2$, and the velocity is determined from the flight time, $v = d/t$. This does not include any attenuation of charge exchange neutrals between the time of their formation and detection.

Fig. 6 shows the distribution function for the detector signal shown in Fig. 5. The data points are shown as asterisks. Also shown in Fig. 6 is an estimate of the noise level of the detector con-
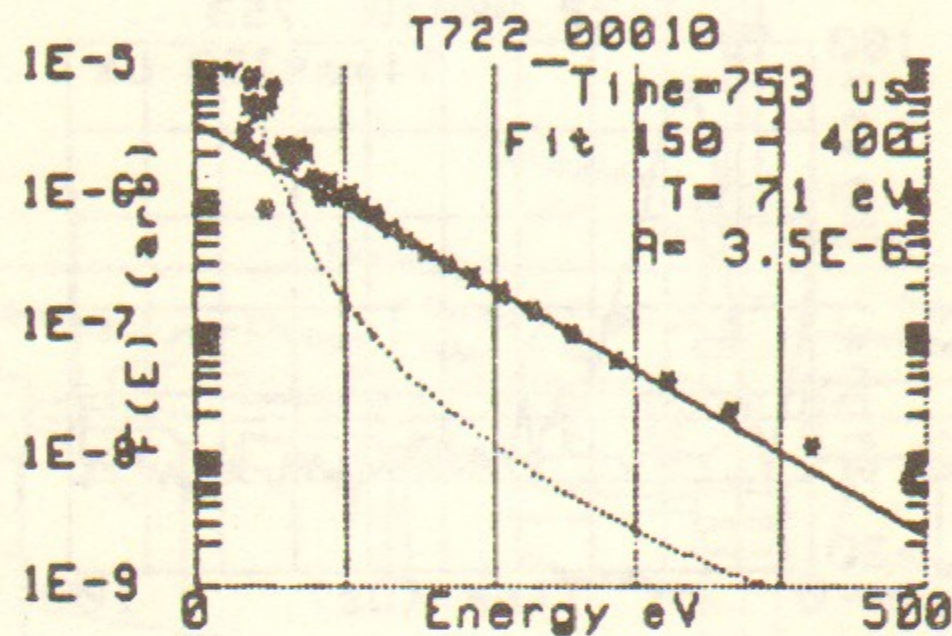

Fig. 6. Ion distribution function for the data in Fig. 5.

verted to a distribution by Eq. (1). This is shown as a dotted line. We find that when the data lies significantly above the noise, the distribution can be fit reasonably well by a Maxwellian distribution with temperature $T = 57$ eV. The least squares best fit to the data is also shown in Fig. 6. In addition to the measurement of the ion temperature, we can also calculate the ion density from the spectra. If we assume the data are well fit by a Maxwellian with temperature T and amplitude A, the ion density is given by the normalization integral of the Maxwellian distribution. The normalization integral is given by

$$ n = \int_0^\infty f(v)\, v^2\, dv , \qquad (2) $$

where $f(v)$ is the best fit distribution function given by

$$ f(v) = A \exp\left(\frac{-mv^2}{2T}\right) . \qquad (3) $$

The density is given by the relation

$$ n_i = A T^{3/2}. \qquad (4) $$

The assumptions used in the determination of the ion density are a constant neutral density and no attenuation of the charge exchange neutrals between their birth and detection by the TOF analyzer.

2. CHARACTERIZATION OF THE AMBAL-U PLASMA

The diamagnetic loop signal, the 4 mm cutoff signal and the 8 mm cutoff signal for a typical discharge in the optimal regime for hot ion capture are shown in Fig. 7. Approximately 1.2 ms after triggering the digitizers, the four plasma guns are fired. The plasma gun parameters for the optimal operating regime were found to be: 10 atm hydrogen gas pressure in the plasma gun gas supply, 3 ms time delay between the gas pulse and the initiation of the discharge, and a solenoid magnetic field of 2.5 kG. The AMBAL-U magnetic field on this discharge was 8 kG at the midplane of the trap. The plasma density in the trap quickly rises as shown by the 8 and 4 mm cutoff signals. At approximately 2 ms, both START injectors are fired. The diamagnetic signal increases about 50% during the START injector pulse. The diamagnetic signal before the START pulse is about $4 \cdot 10^{14}$ eV·cm^{-3}. The average density of trapped plasma as measured by the multicord beam attenuation diagnostic is about 10^{13} cm^{-3}. Data from the beam attenuation diagnostic are shown in Fig. 8. The peak beam attenuation is greater than 15%. This density and diamagnetism correspond to a warm ion temperature of 40 eV.

The increase in the diamagnetic signal during the START injector pulse, as shown in Fig. 7, corresponds to an increase in the diamagnetism to a value of $1.5 \cdot 10^{15}$ eV·cm^{-3}. The shape and location of the diamagnetic loop result in a difference in the sensitivity of the loop to the hot ions and the trapped plasma. The START injector parameters on the discharge shown in Fig. 7 are 18 kV, 100 A total neutral current. The pulse duration of the START injectors is 250 μs. The increase in the diamagnetism during the START pulse is due the trapping of hot ions and the heating of the bulk plasma. The increase in the bulk ion temperature will be discussed in more detail later in this paper. Taking into account the increase in dia-
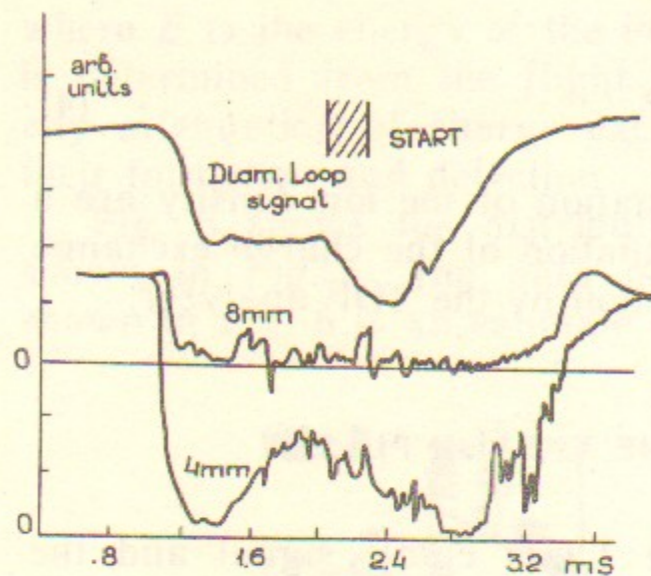
Fig. 7. Diamagnetism, 4 and 8 mm cutoff signals for a shot in the optimal regime. The START injector timing is also shown. The diamagnetic signal increases by 50% during the START pulse.
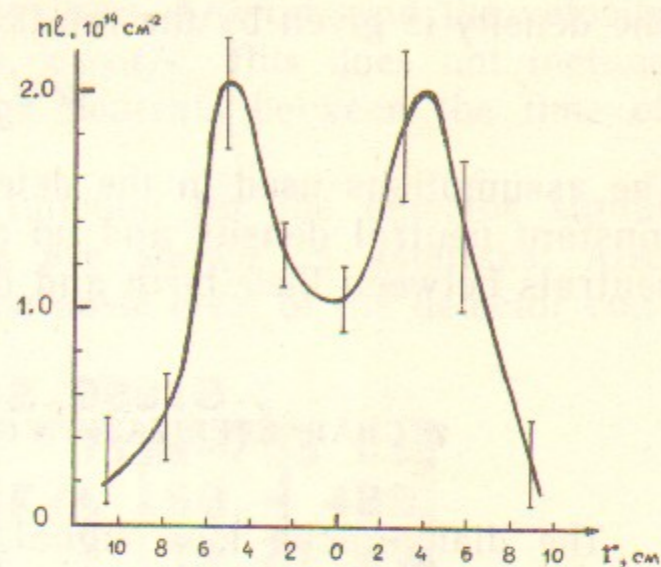

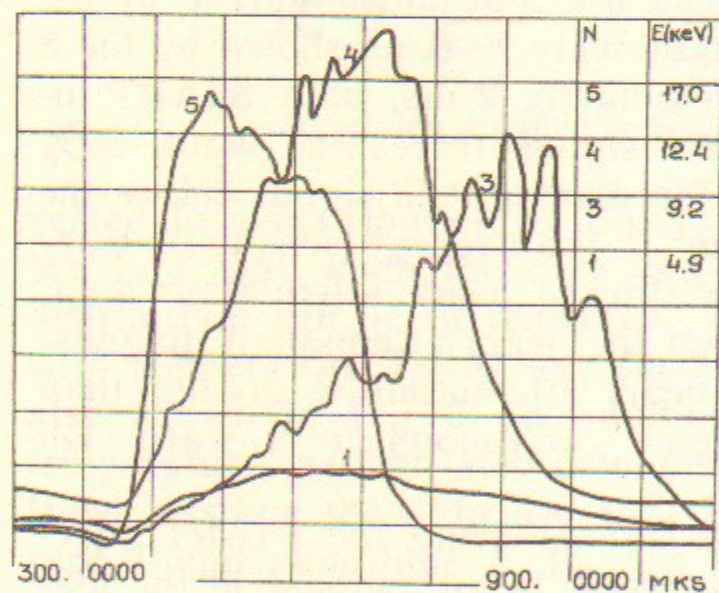Fig. 8. Linear density distribution measured with the beam attenuation diagnostics (BAD).

Fig. 9. Signals from the 5 channel charge exchange analyzer during the START injector pulse. The four signals shown are for energies of 17, 12.4, 9.2 and 4.9 keV.
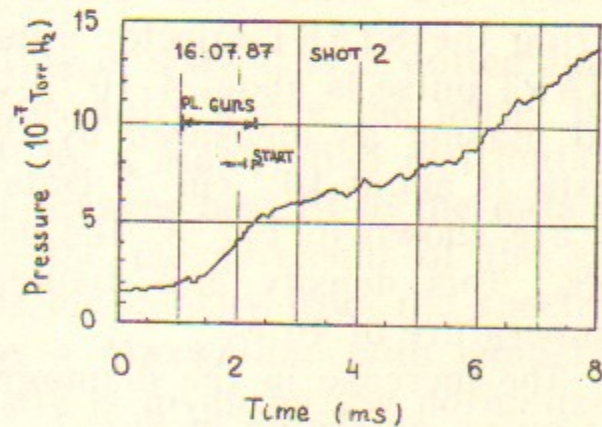
N	E(keV)
5	17.0
4	12.4
3	9.2
1	4.9

Fig. 10. Gas pressure versus time.

magnetism due to heating of the bulk plasma, we find the hot ion density is approximately $1.2 \cdot 10^{11}$ cm^{-3}.

The signals from the five channel charge exchange analyzer during the START injector pulse are shown in Fig. 9. The four channels shown are for energies of 17, 12.4, 9.2 and 4.9 keV. The beam injection energy is 18 keV. The average hot ion energy from the charge exchange analyzer is about 10 keV. The electron drag time can be estimated from the time delay between the peaks in the signals. The electron temperature is found to be between 20 and 30 eV.

Cold gas pressure between the plasma and first wall of AMBAL was measured by fast ion gauges with electron beam modulation and differencing signals of wire collectors. During the plasma pulse pressure in the midplane, at 50 cm from axis usually increased from initial value $5 \div 15 \cdot 10^{-8}$ Torr H_2 up to $2 \div 6 \cdot 10^{-7}$ (Fig. 10).
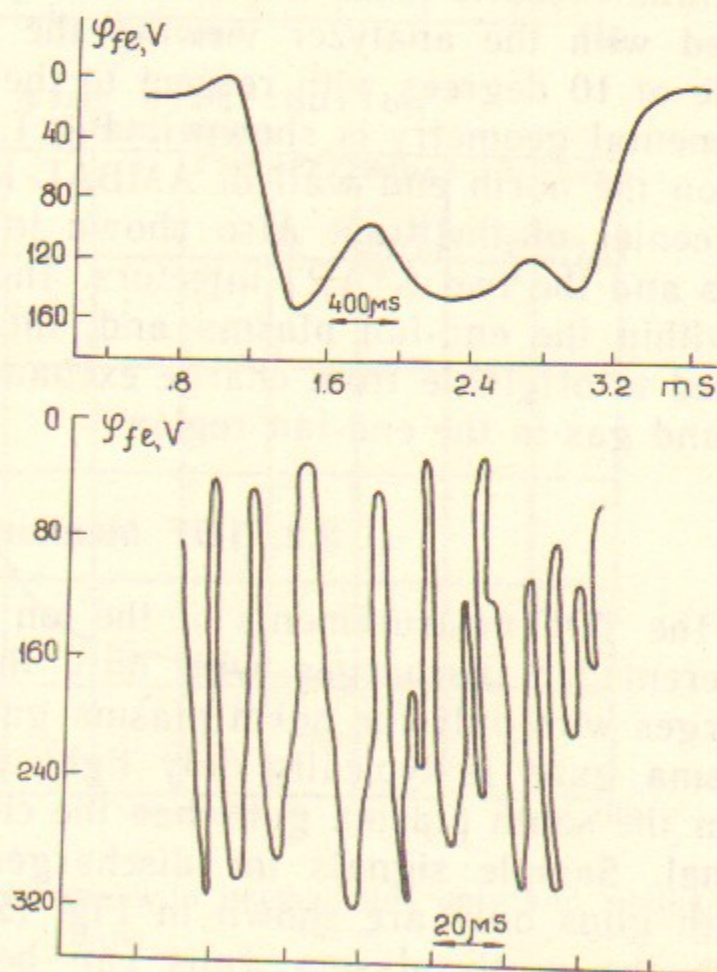

Fig. 11. Mean value of the floating potential measured with a floating potential probe at the midplane of the trap. Also shown is an expanded view of the floating potential showing the high level of rf activity.

The time dependence of the mean value of the floating potential measured by a floating probe at the center of the trap is shown in Fig. 11. Also shown is an expanded view of the RF activity early in the discharge. The oscillations in the floating potential indicate a large amount of RF activity with frequency near 50 kHz. Measure-

ments of the net current to the plasma receiver plates indicate there is a significant amount of nonambipolar radial transport. Total currents incident on the plates can be as high as 1 kA. The existance of the high level of RF activity and the large observed radial transport are believed to be the major limitations on the target plasma. In order to obtain the planned plasma parameters the plasma guns will be moved closer to the mirror peak. This should lead to a reduction in the radial transport rate and an increase in the target density.

3. EXPERIMENTS WITH THE TOF ANALYZER AT 10 DEGREES

3.1. Introduction

Initial results with the TOF analyzer on AMBAL-U were obtained with the analyzer viewing the midplane of the trap at an angle of 10 degrees with respect to the magnetic centerline. The experimental geometry is shown in Fig 1. The TOF analyzer is mounted on the north end wall of AMBAL looking through the mirror at the center of the trap. Also shown in Fig. 1 are the four plasma guns and the two START injectors. The line of sight of the analyzer is within the end-fan plasma and, thus, some of the signal is expected to originate from charge exchange of plasma ions with background gas in the end-fan region.

3.2. TOF Measurements

The TOF measurements of the ion distribution are substantially different for discharges with only the south guns than for discharges with only the north plasma guns. The signal from the north plasma guns is typically only light with no particles. The signal from the south plasma guns has the characteristic light and particle signal. Sample signals for discharges with north guns only and south guns only are shown in Fig. 12. The lack of particle signal from the north plasma guns can be explained in several ways. First, the plasma guns inject plasma along the magnetic field lines of the fan region into the trap. The line of sight of the TOF analyzer and the plasma generated by the north plasma guns may not overlap until near the magnetic field peak. The TOF line of sight overlaps the plasma from the south plasma gun for a much longer
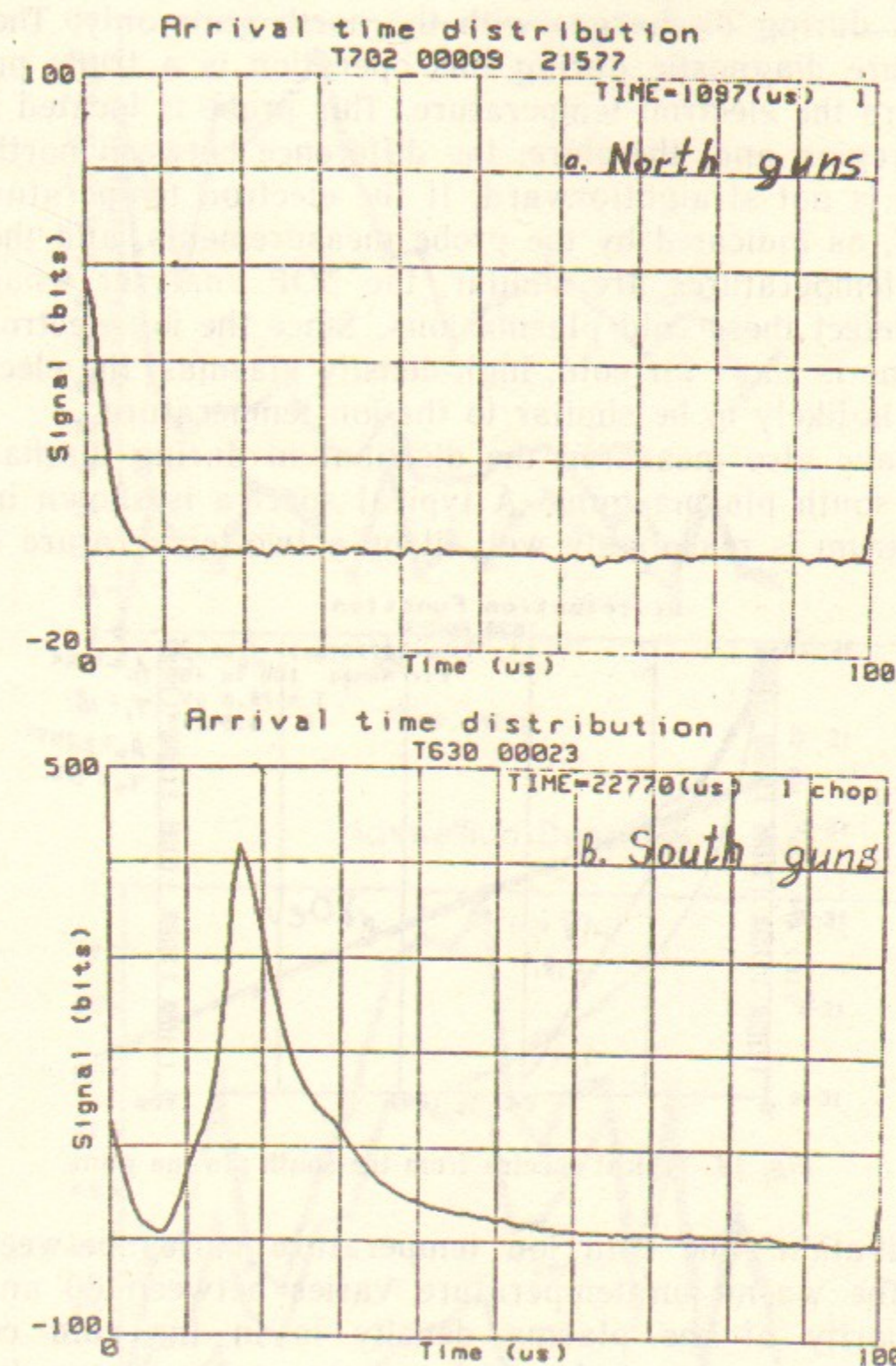
14

Fig. 12. Detector signals from discharges with norths guns only and souths guns only.

15

distance in the fan region. Another explanation for the lack of particle signal from the north guns is the low temperature typically measured during discharges with the north guns only. The primary temperature diagnostic during this operation is a triple probe used to measure the electron temperature. This probe is located in the south fan region and, therefore, the difference between north and south guns is not straightforward. If the electron temperature is only a few eV, as indicated by the probe measurements, and the ion and electron temperatures are similar, the TOF analyzer would not be able to detect these cold plasma ions. Since the ion-electron equilibration time is short for cold, high-density plasmas, the electron temperature is likely to be similar to the ion temperature.

We have also measured the distribution during discharges with only the south plasma guns. A typical spectra is shown in Fig. 13. The spectrum is reasonably well fit by a two-temperature Maxwelli-

Distribution Function
T630 00023

Time=22770(us) 1 chop
Fit Range 100 to 400
T = 79.8 eV
A = 3.84E-5
$A_1 = 7.44$
$T_1 = 18$
$A_2 = 3.8 H5$
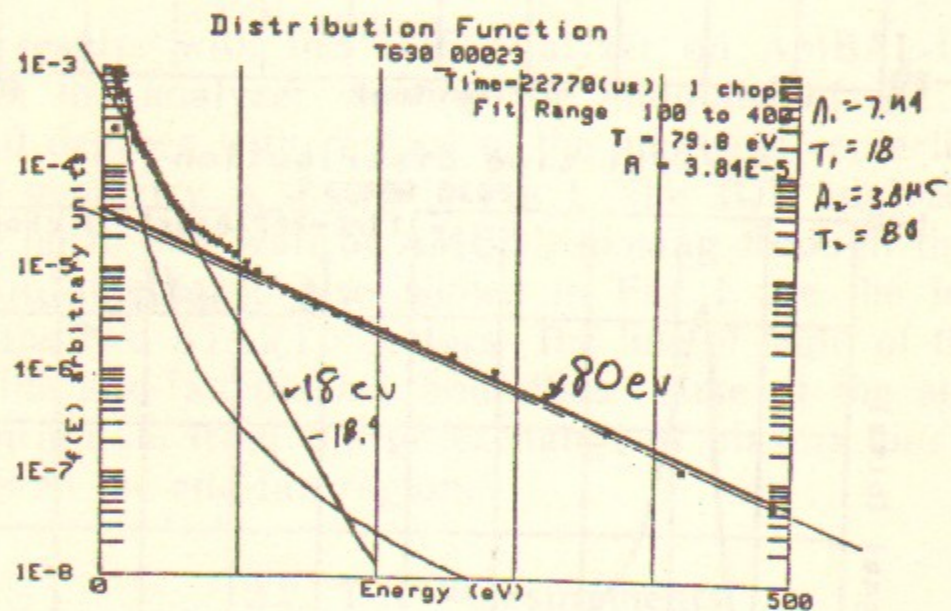$T_2 = 80$

~18 eV ~18.9
~80ev

Fig. 13. Typical spectra from the south plasma guns.

an distribution. The cold ion temperature varies between 10 and 40 eV. The warm ion temperature varies between 60 and 140 eV. The majority of the plasma density is in the cold component. Fig. 14 shows a plot of the cold and warm ion temperature versus time. Also shown in Fig. 14 is a plot of the cold, warm, and total ion density versus time. We find that the warm ion temperature is typically larger early in the discharge. The temperature then falls .5 to 1 ms into the shot. We find that the variations in the ion temperature agree well with the data obtained on the plasma gun test facility [12].

The effect of the START beam pulse on the target plasma has

16

Maxwellian Temperatures

T_{warm}
T_{ave}
T_{cold}
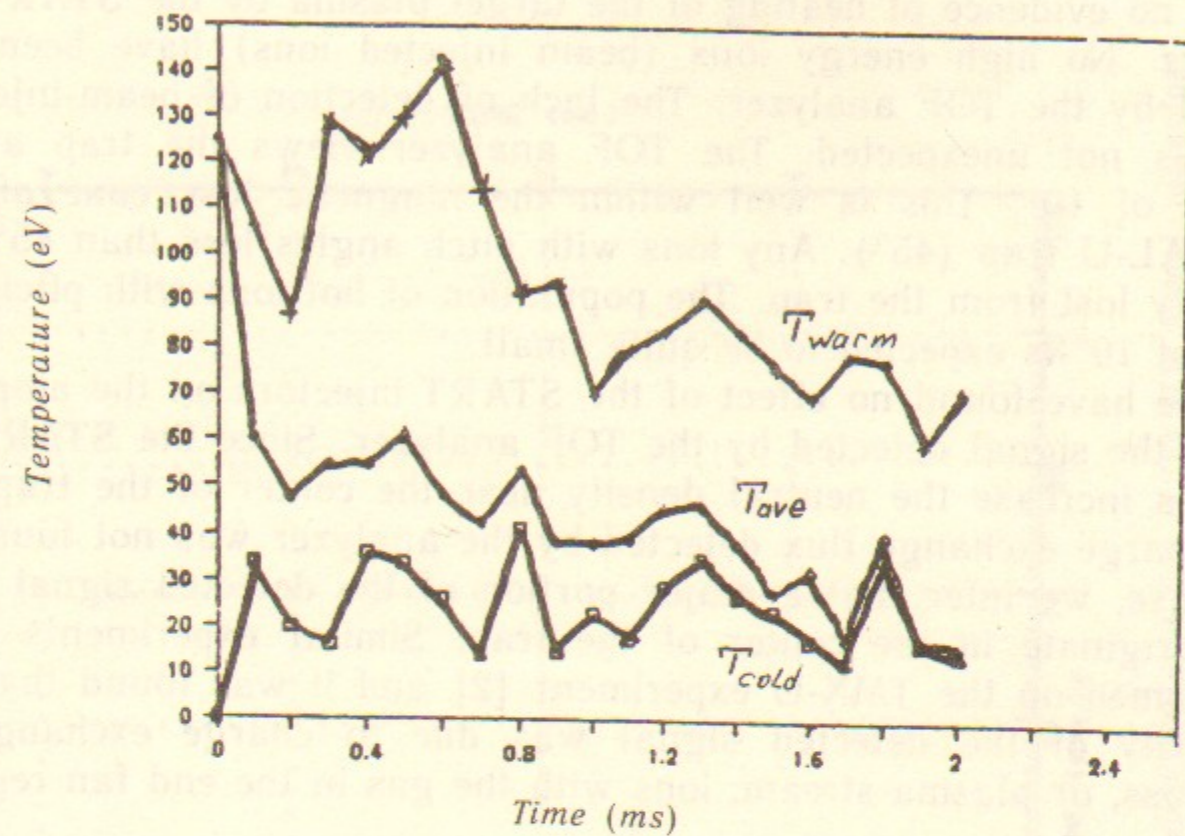
Maxwellian Densities
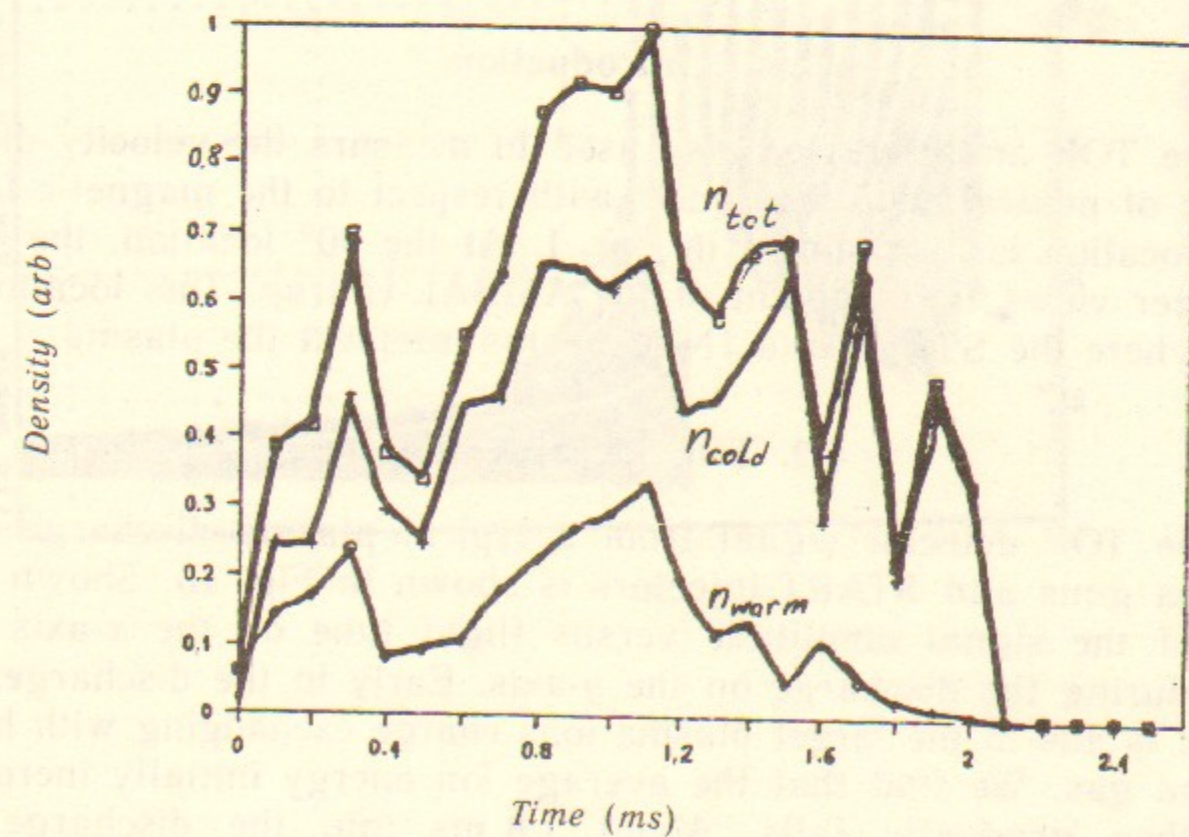
n_{tot}
n_{cold}
n_{warm}

Fig. 14. Cold and warm ion temperature vs. time (10 deg.) south guns.

17

also been studied. The TOF measurements of the distribution at 10° show no evidence of heating of the target plasma by the START injectors. No high energy ions (beam injected ions) have been detected by the TOF analyzer. The lack of detection of beam-injected ions is not unexpected. The TOF analyzer views the trap at an angle of 10°. This is well within the magnetic loss cone of the AMBAL-U trap (45°). Any ions with pitch angles less than 45° are quickly lost from the trap. The population of hot ions with pitch angles of 10° is expected to be quite small.

We have found no effect of the START injectors on the amplitude of the signal detected by the TOF analyzer. Since the START injectors increase the neutral density near the center of the trap but the charge exchange flux detected by the analyzer was not found to increase, we infer that a major portion of the detected signal does not originate in the center of the trap. Similar experiments were performed on the TMX-U experiment [2] and it was found that the majority of the detected signal was due to charge exchange of end-loss, or plasma-stream, ions with the gas in the end fan region.

4. EXPERIMENTS AT 90 DEGREES

4.1. Introduction

The TOF analyzer was also used to measure the velocity distribution of neutrals emitted at 90° with respect to the magnetic field. This location is also shown in Fig. 1. At the 90° location, the TOF analyzer views the midpoint of the AMBAL-U trap. This location is also where the START and INAC beams intersect the plasma.

4.2. TOF Measurements

The TOF detector signal from a typical plasma discharge with plasma guns and START injectors is shown in Fig. 15. Shown is a plot of the signal amplitude versus flight time on the x-axis and time during the discharge on the y-axis. Early in the discharge, the signal is due to the target plasma ions charge exchanging with background gas. We find that the average ion energy initially increases but then gradually falls. About 1.8 ms into the discharge the START injectors are fired for approximately 200 μs. The signal from the START injectors can be seen as very high energy particles
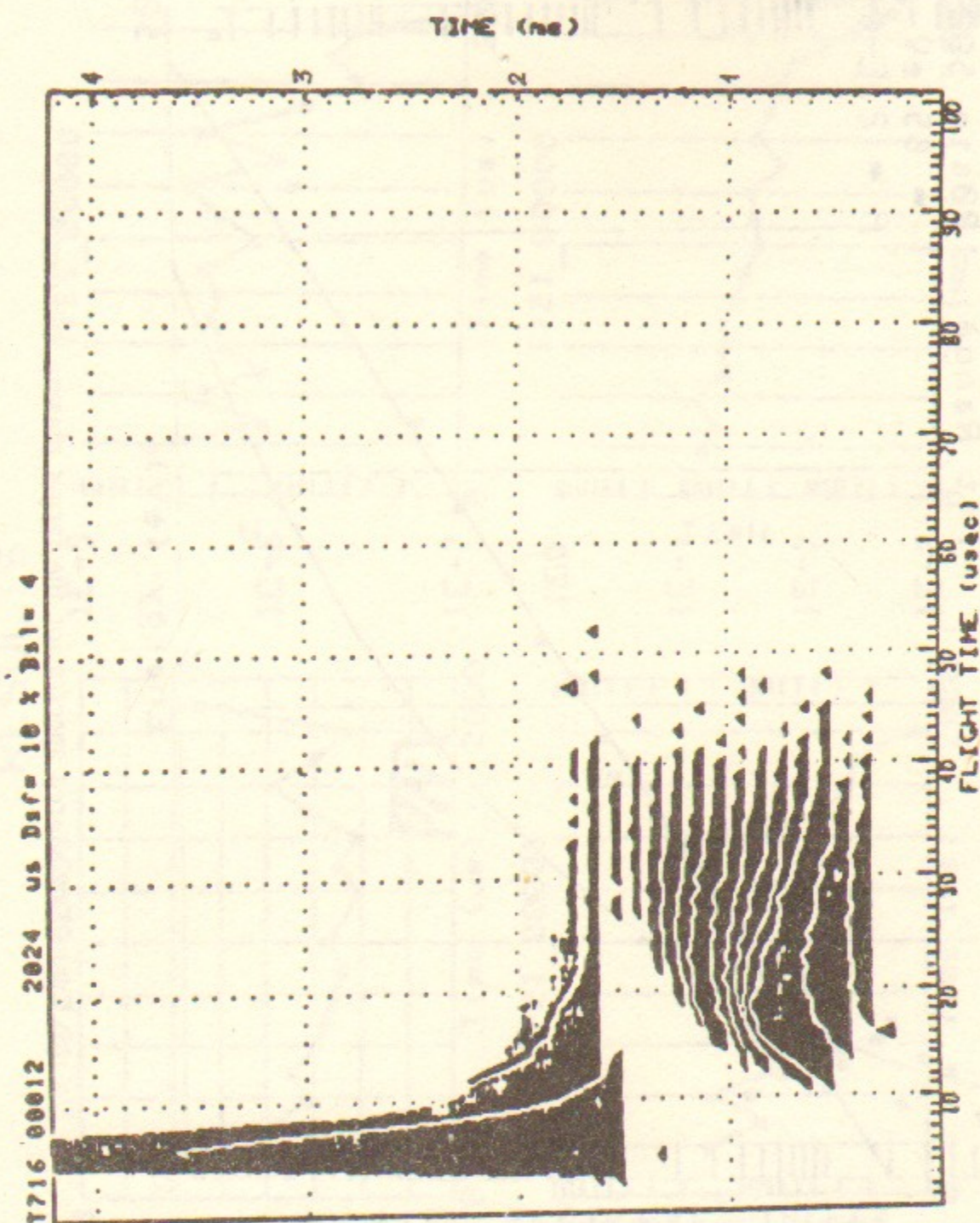
18

Fig. 15. Typical TOF signal at 90 degrees showing time evolution of the TOF signal, including target plasma and START injectors.
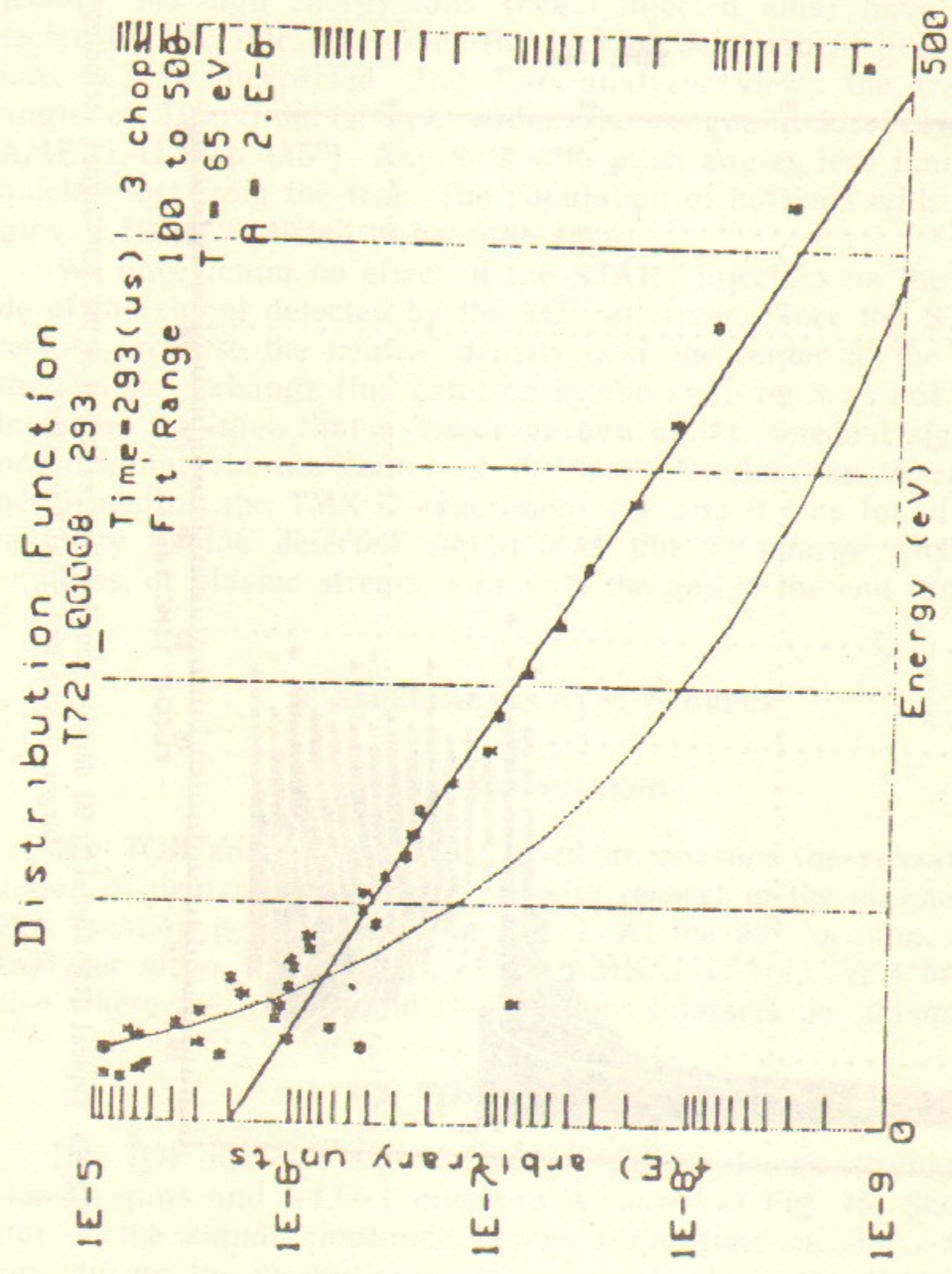
19

Distribution Function
T721_00008 293
Time=293(us) 3 chop
Fit Range 100 to 500
T = 65 eV
A = 2.E-6

Fig. 16. Typical measured spectra for the target plasma (90 degrees).
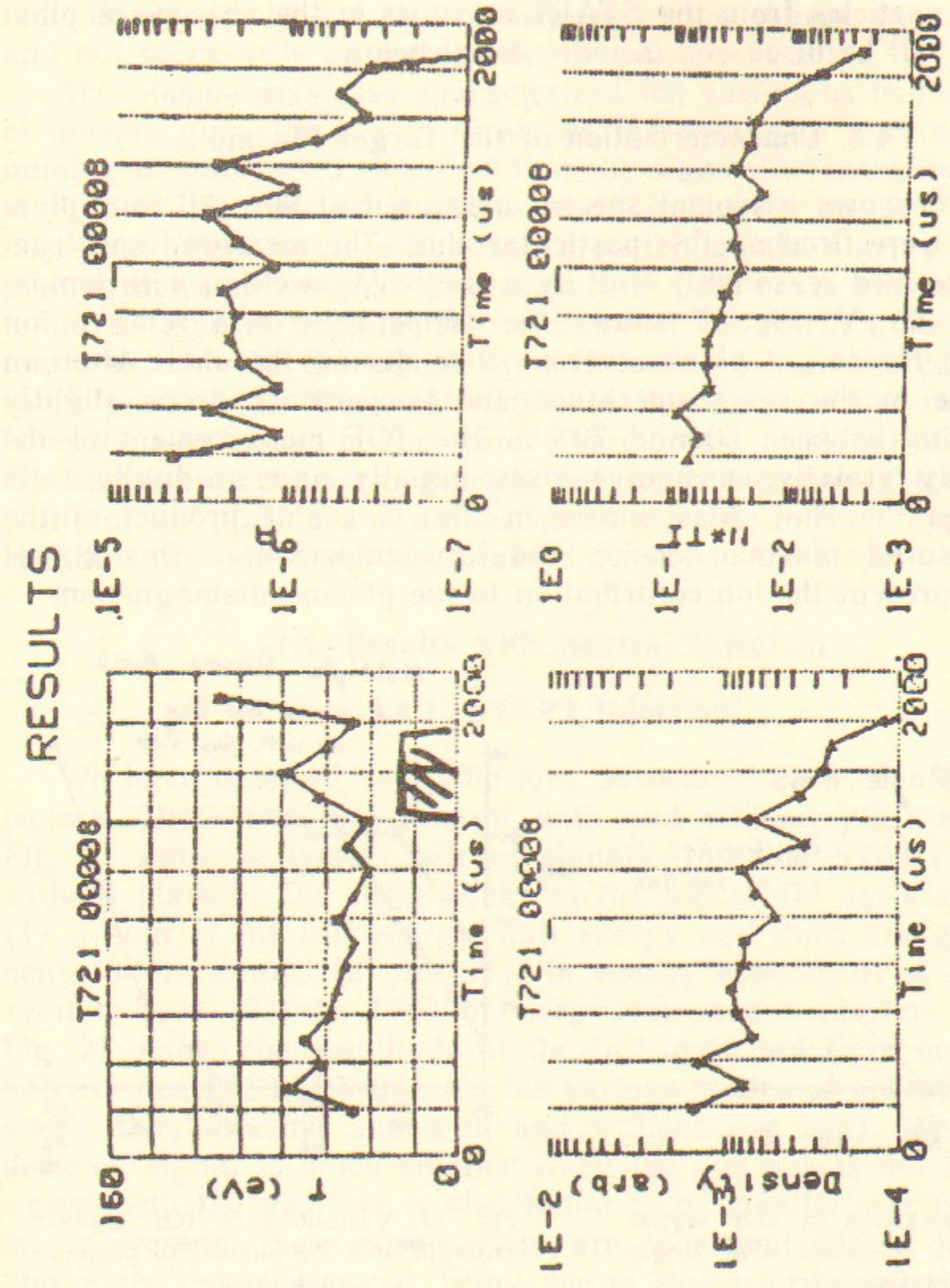
RESULTS

Fig. 17. Time evolution of the TOF measured temperature, density and the product of density and temperature.

(small flight times) late in the discharge. We also have detected energetic particles from the START injectors in the absence of plasma. This will be discussed in more detail below.

4.3. Characterization of the Target Plasma

Fig. 16 shows a typical spectra measured at 90°. All four plasma guns were fired on this particular shot. The measured spectrum is characterized reasonably well by a single Maxwellian with temperature of 65 eV. Fig. 17 shows the temperature and relative ion density of the target plasma versus time during the shot. After an initial rise in the ion temperature, the temperature drops slightly but remains between 50 and 70 eV. The TOF measurement of the ion density (relative measure) rises initially and gradually falls throughout the shot. Also shown in Fig. 17 is the product of the TOF-measured plasma density and ion temperature. This signal should represent the ion contribution to the plasma diamagnetism.
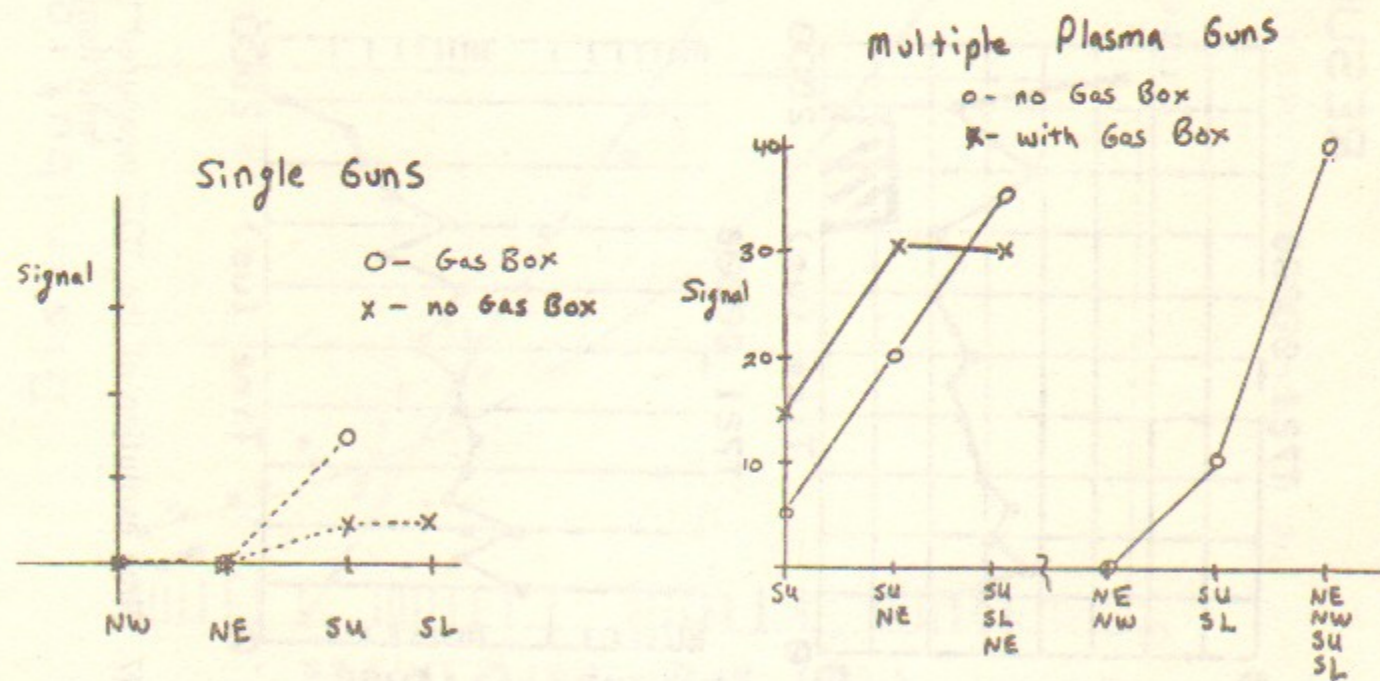

Fig. 18. Variations in TOF signal strength for operation with single plasma guns.

Fig. 19. Variations in TOF signal strength with the number of plasma guns used.

The plasma from each plasma gun was also characterized. The detected signal from the individual plasma guns was also measured. This data is shown in Fig. 18. During operation with either of the north plasma guns, no signal was detected. Operation of the

south plasma guns gave easily detectable signals. The addition of gas from the gas box was also found to increase the detected signal. This is likely due to an increase in the charge exchange rate and not necessarily an increase in the plasma density.

The plasma was also characterized for variations in the number of plasma guns fired. Fig. 19 shows the results of variation in the number of guns used. We find that the signal increases by a factor of 4 from the case of a single south gun with the addition of a north gun. This result is obtained even though the north guns alone give no detectable signal. Operation with both north plasma guns is found to give no signal. The addition of the north guns is again found to increase the signal by a factor of 4 over the case of the south guns alone. One explanation of this data is that the plasma from the north guns is very cold. The increase in signal obtained by the addition of the north guns is due to an increase in the collisionality of the plasma and a subsequent increase in the trapping rate, and thus, an increase in the plasma density in the trap.

4.4. Results with Neutral Injection

4.4.1. START Injection

We have detected energetic ions associated with the START injectors. These ions are present with and without plasma present. Fig. 20 shows a typical pair of signals from the START injectors without plasma. The three peaks in the signal are associated with: (1) a sum of the full energy, half energy and third energy components of the beam, (2) the 1/18'th energy component of the beam (water) and (3) the 1/40'th energy component (carbon dioxide). Fig. 21 shows the amplitude of the full, half and third energy signal from each START injector for various modes of operation (with and without plasma and with and without gas box). We find the detected signal is much smaller when the gas box is not used. The signal with the gas box is also found to be smaller when the plasma is present. These observations are consistent with a large portion of the detected signal, being due to Rutherford scattering of the energetic neutrals from the background gas molecules.

We can estimate the expected increase in ion temperature due to heating of the bulk plasma by the hot START injected ions. There are two major processes to be considered. First is the direct transfer of energy from the hot ions to the bulk plasma. The expression

START with Gas Box
(no plasma)
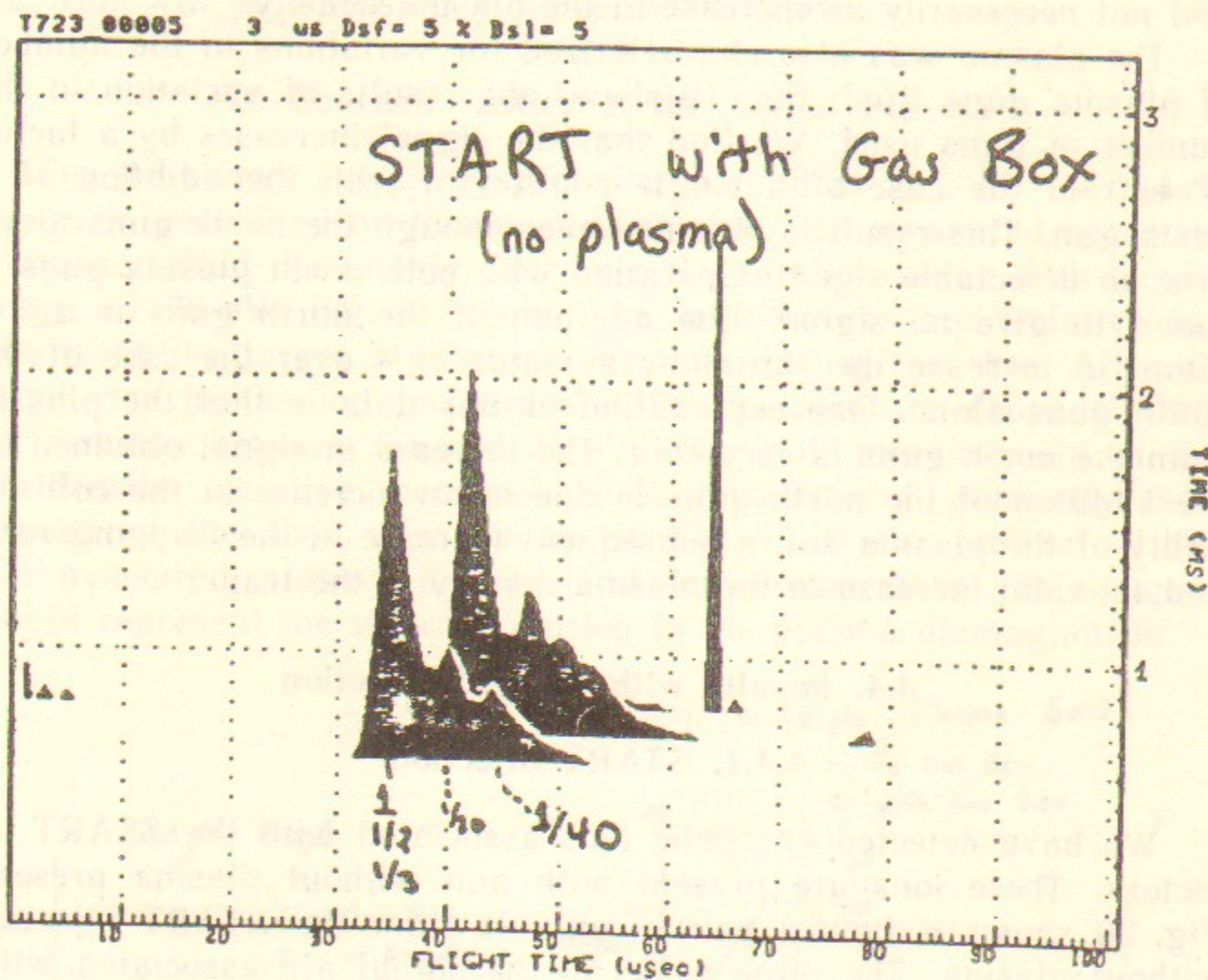
Distribution Function
T723 00005 533

Fig. 20. TOF signal from the START injectors without plasma.

for the temperature rise is given by Spitzer [13]

$$\frac{dT}{dt} = \frac{T_h - T_c}{\tau_{eq}} \qquad (5)$$

where T_h is the hot ion temperature, T_c is the bulk temperature, and τ_{eq} is the energy equilibration time given for hydrogen plasmas by

$$\tau_{eq} = \frac{5 \cdot 10^5 (T_c + T_h)^{1.5}}{n_h} \text{ (s)} \qquad (6)$$

where T_c and T_h are given in eV and n_h is the hot ion density. For typical AMBAL-U parameters ($T_c = 50$ eV, $T_h = 10$ keV, $n_h = 3 \cdot 10^{10}$ cm^{-3}) the energy equilibration time is about 15 seconds. Inserting this into Eq. (4), we find that, for 200 µs START beams, the expected increase in the ion temperature is about .1 eV. This process is not considered important.

Another process for heating the target ions is via electrons. Energy is transferred to the electrons from the hot ions via electron drag. The electrons then equilibrate with the ions, resulting in an increase in the bulk ion temperature. The electron drag time for hydrogen plasmas is given by

$$n\tau_{drag} = 2.2 \cdot 10^7 \, T_e^{1.5} \qquad (7)$$

where T_e is the electron temperature in eV. For typical AMBAL-U parameters ($n = 3 \cdot 10^{13}$ cm^{-3}, $T_e = 50$ eV), the electron drag time is about 250 µs. The energy equilibration time between ion and electron species is given by Book [14].

$$n\tau_{ei} = 2 \cdot 10^7 \, T^{1.5} \qquad (8)$$

where T is the ion and electron temperature in eV (assumed to be nearly equal). We find the energy equilibration time between ion and electron species to be about 250 µs. We can estimate the increase in the bulk ion temperature from the electron power balance. The electron power balance is determined by the following terms

$$\frac{dT_e}{dt} = hot \; ion \; drag - warm \; ion \; drag - loss \; current \times T_e -$$

$$- excitation - ionization . \qquad (9)$$

For simplicity, we will neglect the energy loss due to excitation and

ionization reactions. We can estimate the ratio of the two remaining loss processes from the electron ion equilibration rate and the plasma confinement time. We find that the warm ion drag time is about half the plasma confinement time and, thus, 2/3 of the additional energy in the electrons should be transferred from the electrons to the ions and 1/3 to the end wall.

Using Eq. (5), we can estimate the increase in the ion temperature via the electron drag and equilibration processes. We find that for 200 μs beams we expect 5—10 eV increase in the ion temperature, assuming the electron and ion temperature rise together. We feel that in practice this can be considered an upper limit on the expected temperature increase.

Fig. 17 shows the temperature of the warm ions in the trap as a function of time. Late in the shot (at 1.4 ms) the START injectors are fired. The TOF analyzer shows an increase in the warm ion temperature of about 30 eV, from 45 eV to 75 eV. Typical increases are in the range of 5 to 15 eV.
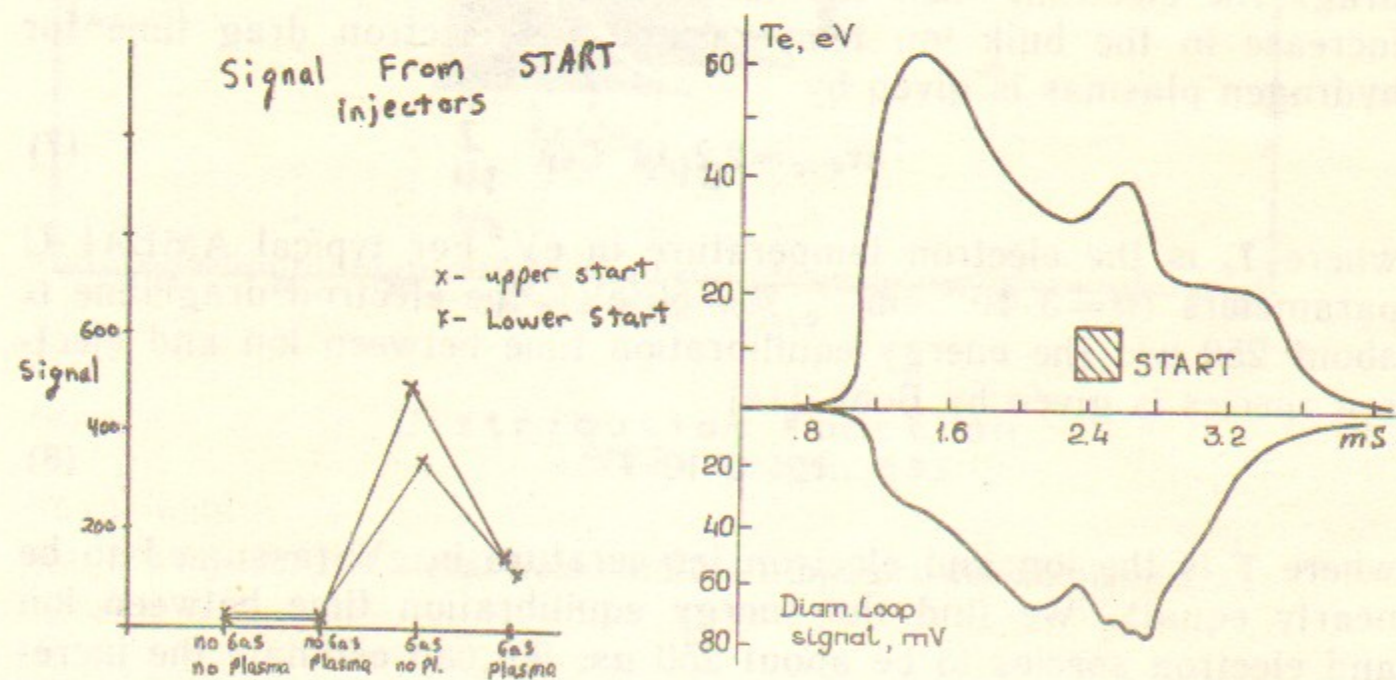

Fig. 21. Signal from the START injectors under various operating conditions.

Fig. 22. Electron temperature in the south fan as measured by the triple probe. The electron temperature increases from 30 to 40 eV during the START injector pulse.

Fig. 22 shows electron temperature measurements made with the triple probe in the south fan tank on a similar shot. The electron temperature reaches a peak of about 60 eV early in the discharge.

When the START injectors fire 2.4 ms after the digitizers trigger, the electron temperature increases from 30 to 40 eV. This increase is consistent with the increase in the ion temperature measured by the TOF analyzer.

4.4.2. INAK Injection

The TOF analyzer has also been used to measure energetic particles from the INAK injectors. Very high energy particles have been detected by the analyzer when the INAK beams are fired into the target plasma. Fig. 23 shows a typical signal obtained from the injection of the INAK beam into the target plasma. Although the resolution
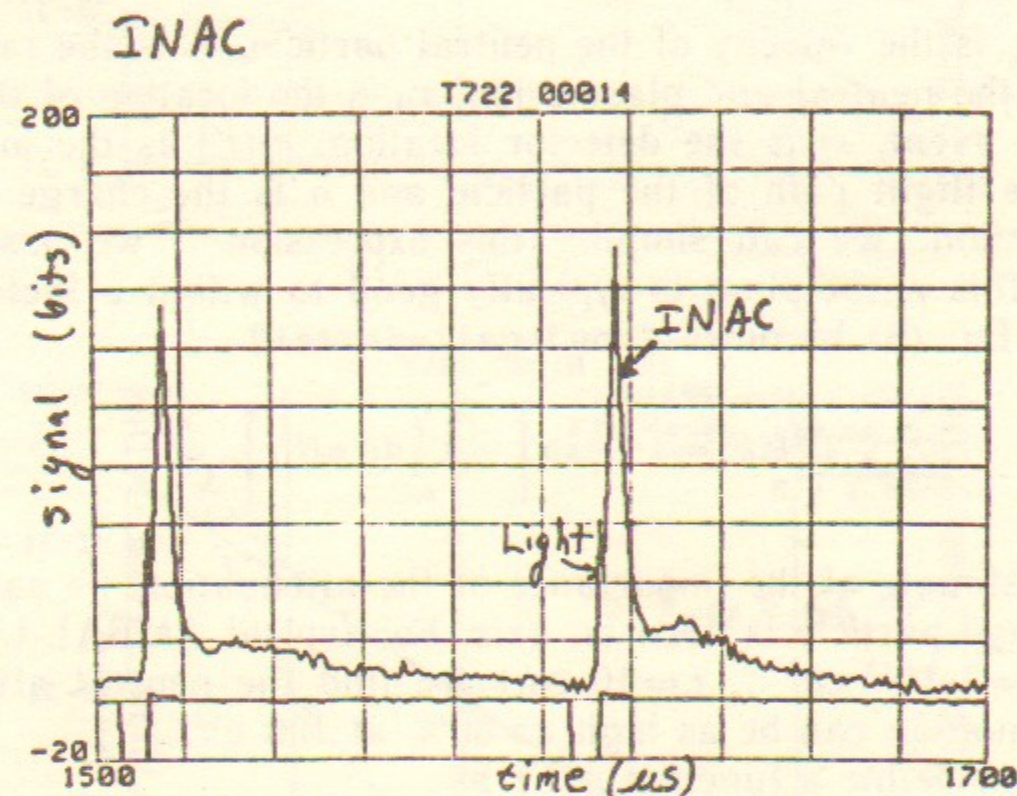

Fig. 23. Signal from the INAK beams fired into the target plasma.

solution of the TOF is very poor at these energies, we find the particles are near the range of the beam injection energy. In the absence of plasma, the TOF detects no signal from the INAK beams. This indicates that a fraction of the INAK neutrals are trapped by the plasma charge exchange and are subsequently detected by the TOF. No signal has been detected due to neutral particle reflection from the INAK beam dump. Although the current delivered to the plasma from the INAK beam is much smaller than that from the START injectors, the TOF analyzer detects about 1/3 to 1/5 as much signal from the INAK as from the START injectors.

4.5. Neutral Attenuation

Attenuation of charge exchange neutrals as they travel from their origin to the TOF detector can be significant, especially when the plasma density is large. The dominant loss mechanism is charge exchange of the neutrals with plasma ions before the neutrals can escape from the plasma. The attenuation probability for a neutral is given by the relation

$$P(E) = 1 - \exp\left[-\frac{1}{v_{H_0}} \int_{x_0}^{x_f} dl'\, n_i(l') \langle \sigma v_r \rangle \right] \qquad (10)$$

where v_{H_0} is the velocity of the neutral particle, v_r is the relative velocity of the neutral and plasma ion, x_0 is the location of the charge exchange event, x_f is the detector location, $n_i(l')$ is the ion density along the flight path of the particle and σ is the charge exchange cross section. We can simplify this expression if we assume that $v = v_{H_0}$. This assumption is typically good to within a factor of 2 if $E_{H_0} > T_i$. Eq. (8) becomes

$$P(E) = 1 - \exp\left[-\sigma \int_{x_0}^{x_f} dl'\, n_i(l') \right]. \qquad (11)$$

For an estimate of the importance of the attenuation we can assume the average particle is born on axis. For typical AMBAL-U parameters $(n_e = 3 \cdot 10^{13}\ cm^{-3},\ r = 10\ cm)$ we find the neutral attenuation. The attenuation can be as high as 80% at 100 eV.

We can define a function $y(E)$ as

$$y(E) = 1/(1 - P(E)). \qquad (12)$$

We can then calculate the actual distribution of emitted neutrals, including the effect of the attenuation of these neutrals before detection. The actual emitted distribution is given in terms of the measured distribution as

$$F(E)_{actual} = y(E)\, F(E)_{measured}. \qquad (13)$$

For simplicity in the computations, we can fit the function $y(E)$ with a power law scaling. We find, for $ndl = 5 \cdot 10^{14}$ and $v_{H_0} = v$, $y(E)$ is reasonably fit by the function.
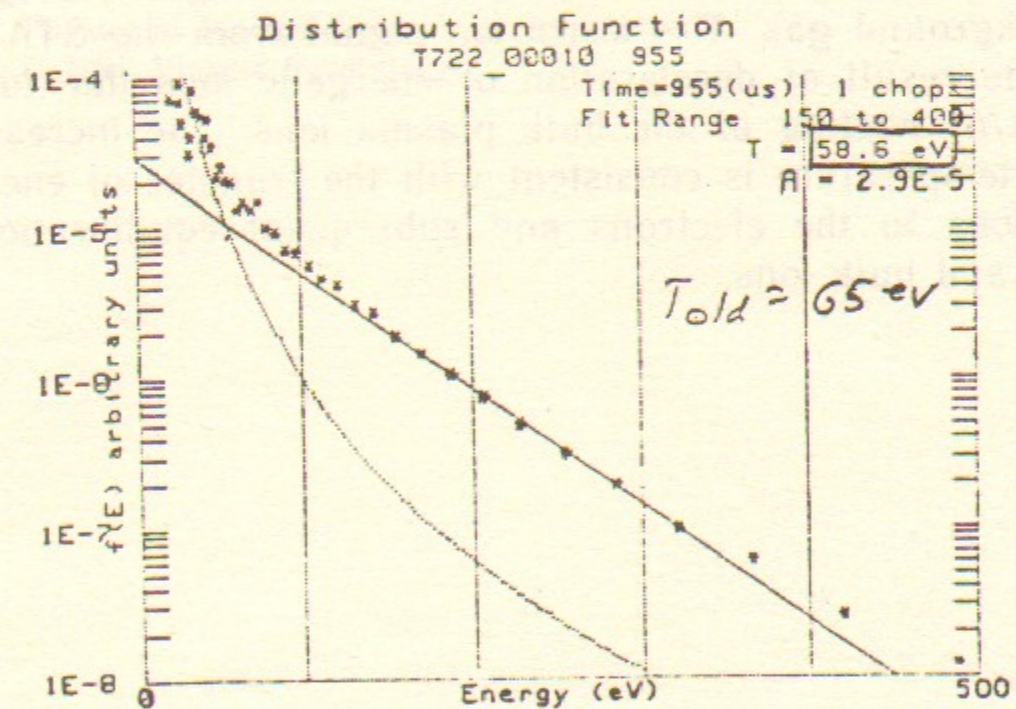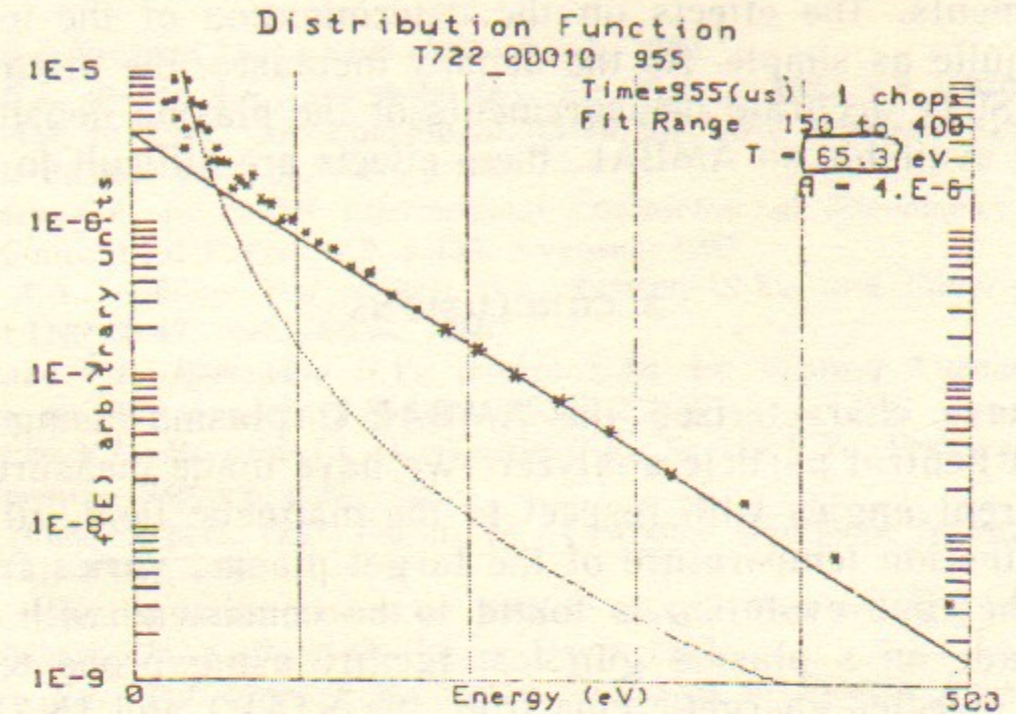
$$y(E) = 37.5\, E^{-.38}. \qquad (14)$$

Fig. 24. The effect of neutral attenuation on the determination of the ion temperature.

Fig. 24 shows the effect of the attenuation on the determination of the ion temperature. The top portion shows the spectrum before the correction for the attenuation effects. The ion temperature is 65 eV. The bottom portion of Fig. 24 shows the spectrum including the effects of attenuation. The correction results in a decrease in the ion temperature to 58 eV. This is about a 10% effect on the temperature

measurements. The effects on the determination of the ion density are not quite as simple. As the density increases, the attenuation increases. Since accurate measurements of the plasma density are not regularly available on AMBAL, these effects are difficult to evaluate.

5. CONCLUSIONS

We have characterized the AMBAL-U plasma using a Time-of-Flight neutral particle analyzer. We have made measurements at two different angles with respect to the magnetic field, 10 and 90°. We find the ion temperature of the target plasma varies from 50 to 70 eV. The time evolution is found to be consistent with measurements made on a plasma gun test facility using probe techniques. We have detected energetic ions from the START and INAK neutral beam injectors. The majority of the hot ion signal from the START injectors is consistent with Rutherford scattering of energetic ions from background gas. The warm ion signal from the START injectors is the result of deceleration of energetic ions due to electron drag and/or heating of the bulk plasma ions. The increase in the bulk ion temperature is consistent with the transfer of energy from the hot ions to the electrons and subsequent equilibration of the electrons and bulk ions.

REFERENCES

1. *Dimov G.I.* Preprint INP 80-152. Novosibirsk, 1980.
2. *Dimov G.I., Ivanov A.A., Roslyakov G.V.* Fiz. Plazmy, 1982, v.8, p.970.
3. *Ivanov A.A.* In: Proc. Cours on Mirror Based and Field Reversed, Approaches to Magnetic Fusion. Varenna, 1983, p.193.
4. *Kabantsev A.A.* In: XVIII International Conference on Phenomena in Ionized Gases. Contributed Papers, v.2, p.430. Swansea, 1987.
5. *Ivanov A.A., Sokolov V.G., Fiksel G.I., Taskaev S.Yu. and Chupriyanov V.E.* Preprint INP 86-47. Novosibirsk, 1986.
6. *Davydenko V.I., Roslyakov G.V., Savkin V.Ya.* In: Voprosy Atomnoy Nauki i Techniki, ser. Termoyadernyj Syntez, 1983, v.2, p.87.
7. *Davydenko V.I., Morozov I.I., Roslyakov G.V., Savkin V.Ya.* Prybory i Technika Eksperimenta, 1986, v.6, p.39—42.
8. TMX-U Final Report, G.D. Porter, ed., Lawrence Livermore National Laboratory, UCID-20981, 1987.
9. Plasma Potential Measurements on TMX-U using a Time-of-Flight Neutral Particle Analyzer, University of California, Davis, 1987.
10. *Freeman R.L. and Jones E.M.* Atomic Processes in Plasma Physics Experiments.—Culham Laboratory, Abingdon, Berkshire, 1974.
11. *Ivanov A.A., Kabantsev A.A., Roslyakov G.V. and Taskaev S.Yu.* Preprint INP 86-77. Novosibirsk, 1986.
12. Spitzer, Physics of Ionized Gases.
13. *Book D.L.* NRL Plasma Formulary.

M.Carter, D.Behne, S.Hulsey, A.Molvik, G.Porter,
Y.Belchenko, E.Gilev, V.Davydenko, G.Dimov,
V.Dudnikov, A.Kabantsev, V.Karliner, I.Morozov,
V.Sokolov, S.Taskaev, G.Fixel, V.Chupriyanov

Experiments with the Time-of-Flight
Neutral Particle Analyzer on AMBAL-U

М.Картер, Д.Бен, С.Халси, А.Молвик, Г.Портер,
Ю.Бельченко, Е.Гилев, В.Давыденко, Г.Димов,
В.Дудников, А.Кабанцев, В.Карлинер, И.Морозов,
В.Соколов, С.Таскаев, Г.Фиксель, В.Чуприянов

Эксперименты с времяпролетным анализатором
нейтральных частиц на «АМБАЛ-Ю»